DOI: https://doi.org/10.37434/tpwj2026.04.01

EFFECT OF PROCESS PARAMETERS OF THE ADDITIVE ELECTRON BEAM PROCESS ON THE PROPERTIES OF THIN-WALLED PRODUCTS FROM VT6 ALLOY

V.A. Matviichuk, V.M. Nesterenkov, M.O. Sysoev

E.O. Paton Electric Welding Institute of the NASU
11 Kazymyr Malevych Str., 03150, Kyiv, Ukraine

ABSTRACT

The subject of investigation is the process of structure formation and mechanical properties of thin-walled products fabricated by additive electron beam melting (EBM) technology from VT6 titanium alloy (Ti–6Al–4V) powder. The alloy is widely used in industry due to its high weldability, strength, and fatigue resistance. Spherical VT6 titanium alloy powder with a particle size of 40–160 μm, produced by rotary plasma atomisation, was used as feedstock. A computer model was created in Materialise Magics software, from which 36 specimens were printed at beam travel speeds ranging from 500 to 6000 mm/s. It was established that a beam travel speed of 500 mm/s combined with an energy density of 40 J/mm³ ensures complete melting of the powder layer, stable shape formation, and controlled thermal conditions. This promotes the formation of a balanced (α+β)-microstructure with acicular α-phase morphology and α-lamella thickness of 0.5–1.5 μm. The volume fraction of α-Ti is 90±3 %, β-Ti — 10±3 %. The microhardness level of the specimens is $HV_{0.1}$ = 3.5±0.7 GPa. The results demonstrate that the combination of high-quality powder feedstock and a rational printing mode ensures high process reproducibility, structural stability, and suitability of the technology for manufacturing thin-walled products.

KEYWORDS: additive technology, electron beam, VT6 titanium alloy, Ti–6Al–4V, thin-walled products, process parameters, microstructure, chemical composition, microhardness

INTRODUCTION

Traditional metal processing methods are often limited in their capability to produce components with complex configurations. This drives the active development of additive technologies, which enable the fabrication of complex-shaped parts with predicted properties [1].

Research on additive manufacturing processes is relevant to modern materials science, production technologies, and mechanical engineering. Its scientific significance is determined by a set of fundamental and applied challenges that remain insufficiently resolved to date. Industry continuously requires new solutions for the fabrication of lightweight, strong, and heat-resistant structures. This is especially true for components made from titanium alloys that operate under high temperatures, variable loads, and aggressive environments [2]. The VT6 titanium alloy of the Ti–6Al–4V alloying system is one of the most widely used in industry due to its combination of high strength, thermal, and corrosion resistance [3]. These properties provide for its broad application in the aerospace, energy, and medical sectors.

In the field of additive manufacturing, intensive development is observed in wire-based technologies — Wire Arc Additive Manufacturing (WAAM), Wire-based Directed Energy Deposition (wire-DED), Laser Metal Deposition (LMD) — as well as powder-based methods such as Selective Laser Melting (SLM) and Electron Beam Melting (EBM) [4]. In [5], thin-walled specimens of Ti–6Al–4V alloy produced by wire-DED were investigated. This method is characterised by limited resolution, which complicates its application for producing thin-walled products with complex geometries. As noted in [6], wire-DED technology has lower shape formation accuracy compared to powder-based methods such as SLM and EBM. These technologies use a laser or electron beam as the energy source, which ensures stable powder melting and precise component geometry. In [7], the mechanical, microstructural, and electrochemical properties of Ti–6Al–4V specimens fabricated by EBM and SLM are compared. It is shown that EBM provides higher strength, uniform elongation, a more favourable microstructure, stable temperature conditions, and operation in a high vacuum environment, which is especially important for chemically reactive titanium alloys [3]. However, the comparative nature of that study did not allow printing parameters to be determined for specific product types. A number of technical issues remain open for further investigation.

In [8], the effect of EBM parameters on the properties of Ti–6Al–4V products was examined. The authors identified process modes ensuring optimal morphology and stable material structure. In [9], the

influence of EBM parameters on the microstructure and microhardness of titanium alloys was studied. It was shown that Ti–6Al–4V forms a dense cast structure with lamellar-acicular α′-phase and a uniform microhardness distribution. However, that study did not cover thin-walled components, which are more sensitive to thermal gradients and local defects.

Previous research demonstrates the advantages of EBM over other methods (SLM, wire-DED), yet leaves open the question of process parameter optimisation for thin-walled products, which are more susceptible to thermal gradients and local defects. Therefore, identifying the patterns governing the influence of EBM parameters on the structure and properties of thin-walled components from VT6 titanium alloy is highly relevant.

Thus, research in this direction has both scientific value — elucidating the mechanisms of structure formation and phase transformations — and practical value — ensuring the production of components with homogeneous structure, stable properties, and high reproducibility under industrial conditions.

THE AIM OF THE STUDY

is to investigate the patterns of thin-walled specimen formation produced by EBM from VT6 titanium alloy powder.

To achieve this aim, the following tasks were set:

- to investigate the surface morphology of thin-walled specimens;
- to determine their macro- and microstructure;
- to investigate chemical and phase composition;
- to measure microhardness;
- to identify printing modes that provide the best structural condition.

THE OBJECT OF INVESTIGATION

is the process of structure formation and mechanical properties of thin-walled products fabricated by EBM from VT6 titanium alloy powder.

MATERIALS AND EQUIPMENT

VT6 titanium alloy powder produced by rotary plasma atomisation of a rod blank on equipment by Multiflex LLC (Ukraine) [10] was used in the study. The powder granules have a spherical shape with diameters of 40–160 μm, ensuring high bulk density, flowability, and uniform melting during printing. The chemical composition of the powder is given in Table 1.

Test specimens were fabricated by EBM using experimental equipment developed at the PWI. A detailed description of the equipment, process parameters, and control algorithms is given in [11, 12].

Printing was carried out in a vacuum chamber at a working pressure of 10^{-2} Pa. The accelerating voltage of the electron beam gun was 60 kV. The sequence of operations, stages of specimen fabrication, and printing process parameters were determined on the basis of prior research [12]. Five electron beam scanning speed modes in the range of 500–6000 mm/s were employed. The choice of this range is both technologically and economically justified, as it provides an optimal combination of product quality and process efficiency. The powder layer thickness was 100 μm; a bidirectional scanning strategy with a trajectory offset step of 0.2 mm was selected, with the scanning direction of each subsequent layer rotated by 90°. The effective

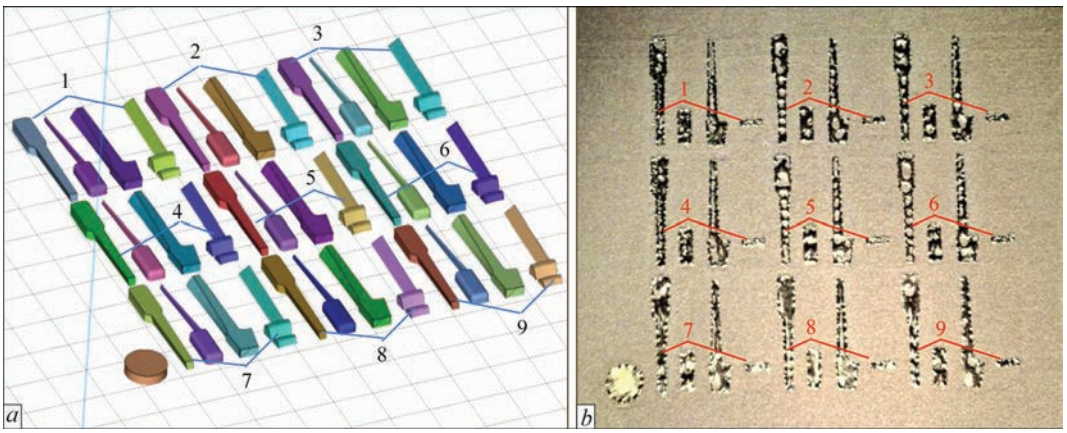

Figure 1. Models and products: *a* — assembly model; *b* — test products, 1–9 — specimen groups

Table 1. Chemical composition of VT6 powder in accordance with TU U 24.4-31914753-001:2018 [10]

Alloying elements, wt.% of particles				Impurities, wt.% of particles			
Al	V	Fe	Ti	O	C	N	H
5.5–6.75	3.5–4.5	≤ 0.3	Base	≤ 0.2	≤ 0.08	≤ 0.05	≤ 0.015

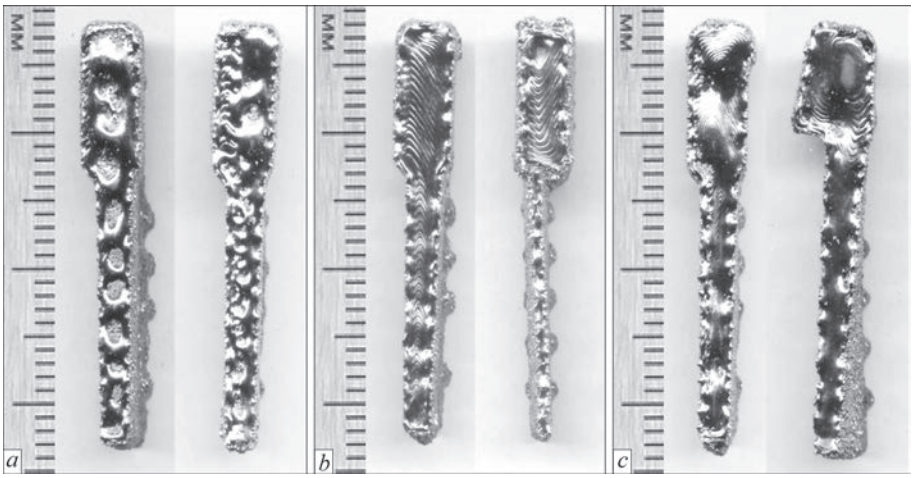

Figure 2. Surface morphology of specimens: *a* — porous; *b* — dense; *c* — bumpy

beam diameter was determined by the dynamic focusing current. Two outer contours were used to improve geometric accuracy [13]. During printing, the powder layer temperature was maintained at 680 °C [12].

A three-dimensional model of the products, incorporating fragments of rotor group components of a gas turbine engine, was created in Materialise Magics. Nine groups of specimens were realised, each corresponding to a separate printing mode (Figure 1, *a*).

A total of 36 specimens (Figure 1, *b*) were printed with the following geometric parameters: length — 30 mm, working section width — up to 2.5 mm, trailing edge thickness — 5 mm, height — 10 mm, of which 5 mm constitute the technological supports. Each of the 9 groups contained 4 specimens produced with varying beam speed, energy density, and focusing.

RESEARCH METHODS

Microstructure investigations were performed using conventional methods. Cross-sectional cuts were made on an electro-discharge machine. Specimens were ground on abrasive paper and polished with diamond suspension. Surfaces were etched in an aqueous solution of 6 % HNO_3 and 2 % HF. Structures were examined using a Carl Zeiss Jena optical microscope. Digital processing of micrographs and quantitative assessment of micro-defects were performed in ImageJ software. Surface topography and phase composition analysis were carried out using TESCAN VEGA 3 SBH EP scanning electron microscope at an accelerating voltage of 20 kV. Chemical composition and element distribution in the metal structure were determined by XRF using Bruker Quantax 610M spectrometer in the atomic number range from magnesium (Z = 12) to uranium (Z = 92). Phase analysis was carried out by X-ray diffraction (XRD) using Inel EQUINOX-1000 diffractometer in grazing incidence geometry at an angle of incidence of 5° to the surface. The X-ray source was a copper anode . Diffraction patterns were recorded in the range 2θ = 30–80° using a radial position-sensitive detector. Experimental data were processed in Match! software. Phase volume fractions were determined by the Rietveld method. Microhardness was measured by the Vickers method using PMT-3 instrument. Tests were conducted at a load of 0.1 kgf (0.98 N) with a dwell time of 10 s. Measurements were performed with a step of 250 μm within the cross-section, with one indentation at each control point.

Table 2. Process printing parameters and surface morphology type of specimens

Group (Figure 1)	Beam parameters				Surface morphology type
	Speed, mm/s	Power, W	Energy density, J/mm³	Dynamic focus current, A	
1	6000	2160	18	0	Porous
2	2000	1000	25	0.83	
3	2000	1000	25	0	
4	4000	1760	22	0	
5	4000	1760	22	0.83	
6	4000	1760	22	0.55	
7	1000	900	45	0	Bumpy
8	500	400	40	0	Dense
9	1000	900	45	1.11	Bumpy

RESULTS AND DISCUSSION

INVESTIGATION OF SPECIMEN SURFACE MORPHOLOGY

The surface condition of the specimens (Figure 1, *b*) was evaluated visually. Initial inspection allowed the specimens to be classified into three types according to surface morphology: porous (Figure 2, *a*), dense (Figure 2, *b*), and bumpy (Figure 2, *c*). The process printing parameters and the corresponding surface morphology type are given in Table 2.

Analysis of the data (Figure 1, *b*; Table 2) showed that the best (defect-free) surface condition corresponds to dense morphology, observed in Group No. 8 specimens printed at a beam speed of 500 mm/s. Bumpy morphology is characteristic of specimens from Groups Nos 7 and 9, produced at a beam speed of 1000 mm/s. Porous morphology with a large number of defects is characteristic of specimens from Groups Nos 1–6, produced at beam speeds in the range of 2000–6000 mm/s.

Based on the data from Figure 1, *b* and Table 2, it was established that surface morphology is significantly dependent on beam travel speed and beam power, whereas the effect of focusing parameters proved to be less significant. The results are explained by the characteristics of thermal processes in the melting zone. At high travel speeds (2000–6000 mm/s), beam power was excessive, leading to excessive heat input and porous surface formation. Bumpy morphology, characteristic of 1000 mm/sspeed may be associated with localised overheating causing surface irregularities. Reducing the speed to 500 mm/s, however, ensures an optimal balance between beam power and speed.

One specimen from each of Groups Nos 1, 3, 4, 7, and 8 (Table 2) was selected for further investigation, covering the full range of speed modes studied.

INVESTIGATION OF SPECIMEN STRUCTURE

In addition to surface condition, the microstructural state is an important material characteristic. Analysis of the microsections (Figure 3) revealed defects in the form of micropores. Defect assessment was carried out by digital processing of micrographs, allowing their number, dimensions, and area to be determined. Measurement results are given in Table 3.

Analysis of Table 3 data established that Specimens Nos 1, 3, and 4 have a significant number of defects — 10 or more — and porous surface morphology (Table 2). The mean defect area was 9124–18294 μm^2 with a mean size of 110–156 μm (Table 3). Specimen No. 7 had a bumpy surface type (Table 2). The mean defect area did not exceed 7775 μm^2 with a mean size of 102 μm. The number of identified pores was only three (Table 3). Specimen No. 8 was characterised by a dense surface (Table 2) with a minimum number of

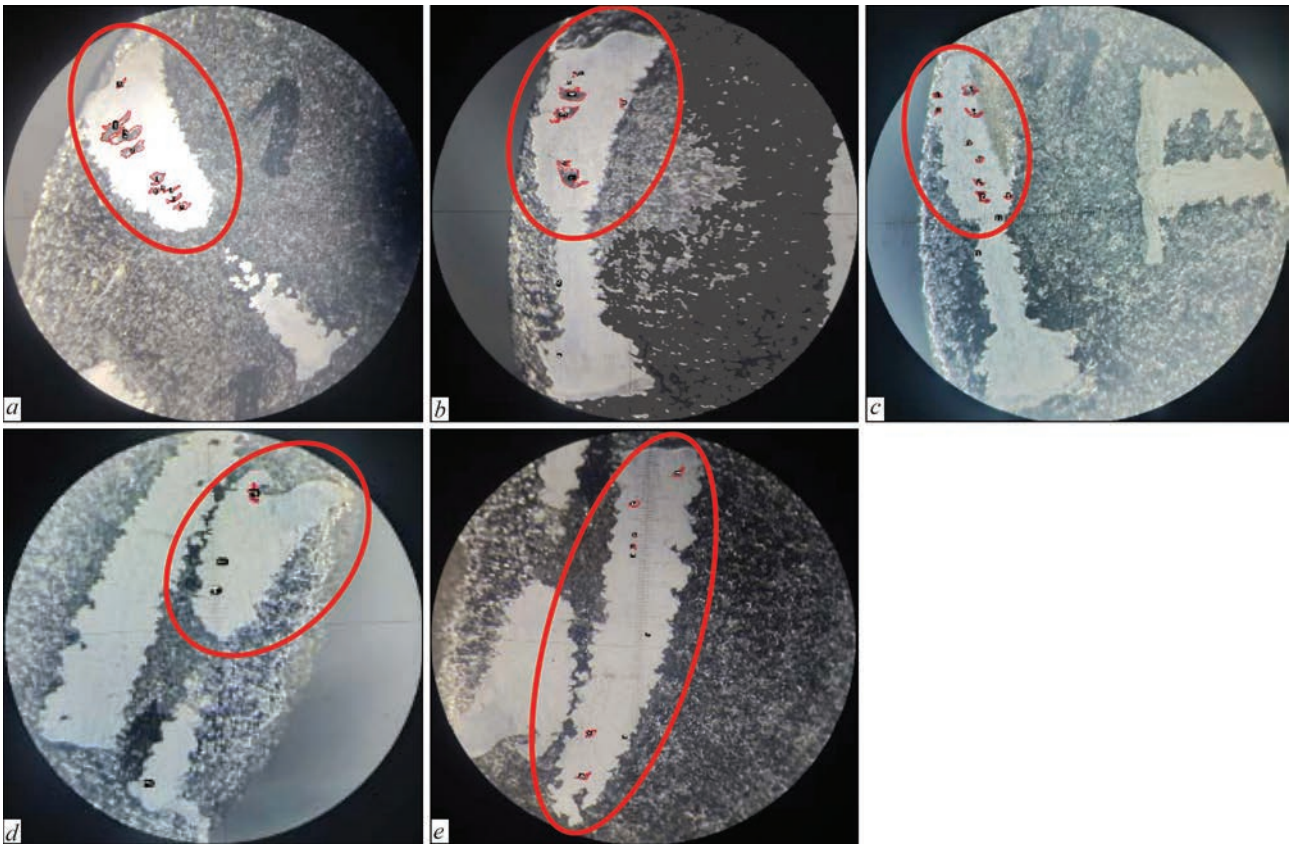

Figure 3. Structures of specimens, No.: *a* — 1; *b* — 3; *c* — 4; *d* — 7; *e* — 8. The area investigated is marked in red

Table 3. Results of internal defect investigations in test specimens

Specimen No. (Figure 3)	Defect area (S) and size (D)						Number of identified defects
	S_{max}, μm²	D_{max}, μm	S_{min}, μm²	D_{min}, μm	S_{av}, μm²	D_{av}, μm	
1	40477	232	3618	69	18294	156	10
3	40454	232	3182	65	14841	141	10
4	17699	154	3022	63	9124	110	11
7	20733	166	2647	59	7775	102	3
8	13064	132	3212	65	7377	99	5

defects — 5 pores — with a mean area not exceeding 7377 μm² and a mean size of 99 μm (Table 3).

The analysis confirmed a clear correlation between surface morphology (Figure 2) and internal defectiveness (Table 3). The increased number and area of defects in specimens with porous morphology indicates that surface condition may serve as an indicator of internal structure. The reduction in defectiveness in Specimens Nos 7 and 8 demonstrates the possibility of optimising printing parameters to achieve a stable structure with minimum defects. Specimens Nos 7 and 8 were selected for further investigation as they exhibit the best surface condition and minimum defect area and number.

Metallographic examination of Specimen No. 7 at ×50 magnification revealed that the metal structure consists of crystallites with different etching degrees, 40–300 μm wide (Figure 4, *a*). The structure demonstrates a pronounced zonality arising from local thermal gradients and non-uniform cooling. At the macro level (Figure 4, *a*), a coarse, non-uniform structure is observed consisting of columnar α-phase crystallites and residual β-phase that did not fully transform. At the micro level (Figure 4, *b*), elongated α-lamellae oriented in one direction are identified, with thin β-phase interlayers between them. This morphology is indicative of martensitic transformation of the β-phase due to rapid cooling in the upper layers. SEM imaging (Figure 4, *c*) confirms the presence of a basket-weave structure with α-lamellae 0.8–1.5 μm thick. Such non-uniformity may result in differences in properties: fine-grained regions with elongated α-lamellae potentially exhibit higher hardness, whereas coarse-grained regions are more prone to local failure due to porosity or microcracks.

Investigation of Specimen No. 8 established that the metal structure at ×50 magnification is more balanced (Figure 4, *d*). It consists of crystallites with different etching degrees, 30–300 μm wide, growing in the direction of the heat flow, while β-phase is partially stabilised in the interlamellar volume. At the micro level at ×500 magnification (Figure 4, *e*), an (α+β)-structure is identified with α-lamellae between which thin β-phase interlayers are located. SEM imaging at ×5000 magnification (Figure 4, *f*) confirms dense packing of α-lamellae 0.6–1.1 μm thick and uniform distribution of the β-phase, forming a balanced (α+β)-morphology (Figure 4, *g*). Such a structure indicates more stable cooling

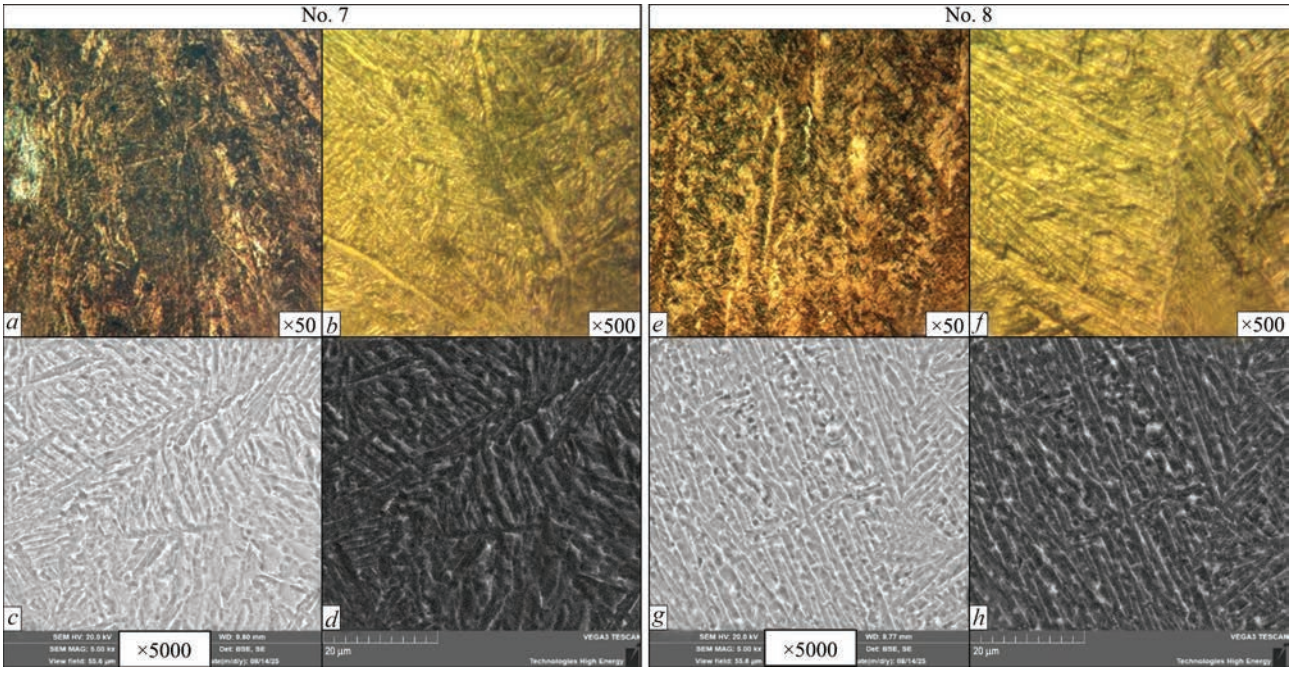

Figure 4. Microstructures of specimens: No. 7 (*a–d*); No. 8 (*e–h*)

Table 4. Chemical composition of specimens (XRF), wt.% (Ti — base)

Designation	Chemical element						
	Mg	Al	Si	V	Fe	Ni	Zr
Specimen No. 7	–	5.059	0.058	4.177	0.102	0.022	0.01
Specimen No. 8	–	5.644	0.062	4.091	0.104	0.046	0.0076
VT6 alloy [14]	≤ 0.30	5.3–6.8	≤ 0.1	3.5–5.3	≤ 0.6	≤ 0.08	≤ 0.30

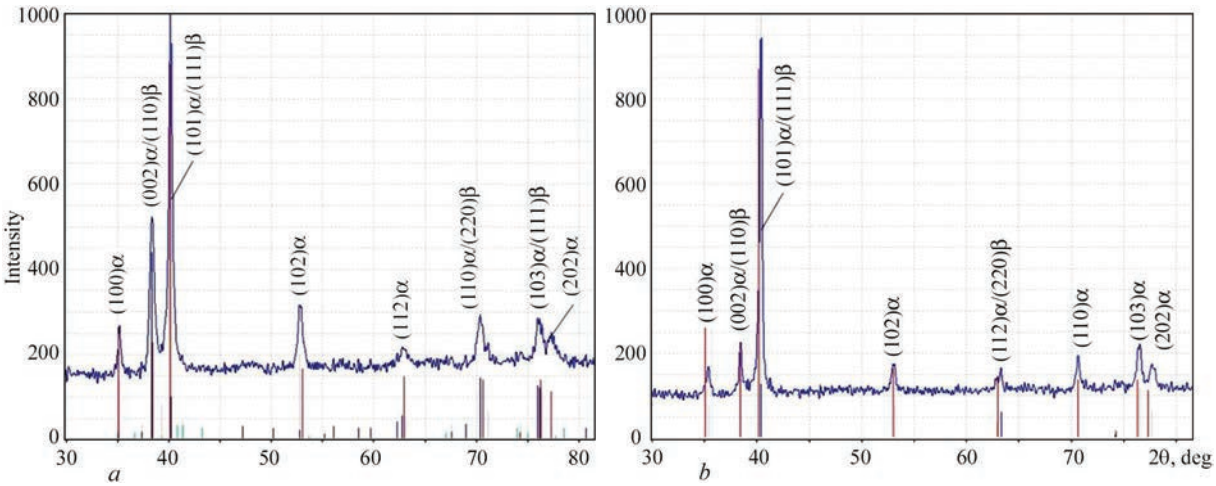

Figure 5. XRD results of specimens: *a* — No. 7; *b* — No. 8

conditions and a more uniform thermal cycle, providing better property homogeneity.

INVESTIGATION OF CHEMICAL AND PHASE COMPOSITION OF SPECIMENS

The investigations showed that chemical composition significantly influences the microstructure of specimens, particularly the Al content, which determines α-phase stability and the phase balance.

According to the data in Table 4, it was established that in Specimen No. 7 the Al concentration (5.059 %) is below the standard range (5.3–6.8 %), which causes a shift in equilibrium towards the β-phase and structural non-uniformity. In Specimen No. 8, the Al content (5.644 %) conforms to the standard, ensuring a stable lamellar α-phase. Thus, Specimen No. 8 has the required chemical composition for the formation of a balanced (α+β)-microstructure, while Specimen No. 7 exhibits phase imbalance due to Al deficiency.

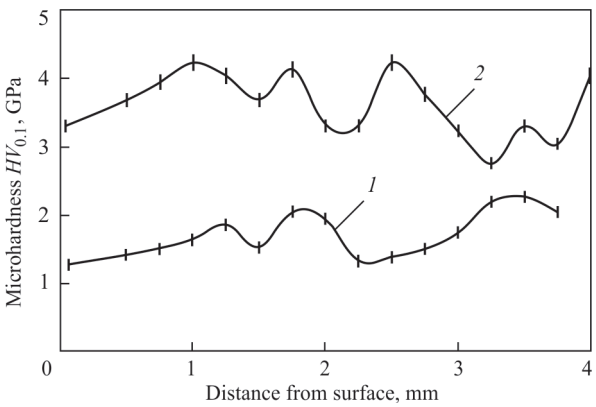

Figure 6. Microhardness ($HV_{0.1}$) variations in specimens, No.: *1* — 7; *2* — 8

X-ray phase analysis allowed the phase composition of specimens to be determined, and the degree of crystallinity, structural purity, and the influence of chemical composition on phase equilibrium to be assessed.

XRD results (Figure 5, *a*) established that Specimen No. 7 exhibits α-phase with a hexagonal close-packed lattice and β-phase with a body-centred cubic structure, where the volume fraction of α-phase is 87±3 % and that of β-phase is 13±3 %. As shown in [15], a reduction in Al content leads to a shift in phase equilibrium towards the β-phase and reduces the morphological stability of the α-phase, which may adversely affect mechanical properties.

Specimen No. 8 demonstrates a clear coincidence of diffraction peaks with reference values (Figure 5, *b*). The intensity and sharpness of the reflections indicate a high degree of crystalline perfection of the phases. This is characteristic of a well-formed α-phase with a volume fraction of 90±3 %. The volume fraction of the β-phase is 10±3 %. The obtained α/β ratio is characteristic of VT6 alloy. As shown in [7] the high crystallinity and the absence of amorphous regions are indicative of a stable thermal crystallisation mode during EBM, ensuring homogeneity of phase composition and improved mechanical properties. This is consistent with the chemical analysis results, where the Al and V content in Specimen No. 8

is within the standard range (Table 4), promoting the formation of a balanced (α+β)-microstructure.

MICROHARDNESS MEASUREMENTS

To evaluate local mechanical properties, microhardness measurements were carried out for Specimens Nos 7 and 8 within the cross-section.

It was established that on the surface of Specimen No. 7 microhardness is $HV_{0.1}$ = 1.3 GPa and it gradually increases, reaching a maximum of $HV_{0.1}$ = 2.3 GPa at a distance of approximately 3.5 mm (Figure 6). This indicates structural non-uniformity of the material, a transition from a less stable surface zone to a more strengthened internal structure. This behaviour is explained by phase instability and reduced Al content, causing local differences in the α/β phase ratio. The mean microhardness of Specimen No. 7 is $HV_{0.1}$ = 1.8±0.5 GPa, which is reduced compared to typical values for VT6 alloy [9].

Specimen No. 8 demonstrates a significantly higher hardness level (Figure 6), ranging from $HV_{0.1}$ = 2.8 to 4.2 GPa. The mean microhardness value is $HV_{0.1}$ = 3.5±0.7 GPa, consistent with characteristic values for VT6 alloy of the Ti–6Al–4V alloying system [9] and indicative of a well-formed (α+β)-microstructure. Hardness fluctuations can be attributed to local features of the thermal cycle, which does not affect the overall structural stability.

DETERMINATION OF PRINTING MODES ENSURING THE BEST STRUCTURAL CONDITION

The results of the comprehensive analysis confirmed that the quality of thin-walled products is significantly dependent on the choice of EBM process parameters. When determining printing modes that ensure the best structural condition, it was established that Specimen No. 8 is distinguished by minimum defectiveness and a balanced microstructure with a uniform phase distribution. Its chemical and phase composition and microhardness values are consistent with the characteristic indicates for VT6 alloy.

Specimen No. 8 was printed at a speed of 500 mm/s and an energy density of 40 J/mm^3. Thus, the implemented process parameters can be considered rational for manufacturing thin-walled products from VT6 alloy. The obtained results are consistent with data from [7], where it is noted that optimisation of beam speed and energy in the EBM process is key to forming a fine-grained microstructure with a minimum defect level.

Despite the positive results obtained, the study has a number of limitations. In particular, the printing parameters were investigated for only one powder type. Microstructure analysis was carried out locally, without accounting for scale effects and complex product geometry. Furthermore, microhardness was used as an assessment of local mechanical behaviour without conducting a full range of mechanical tests. These aspects should be considered in the practical application of the obtained recommendations, as well as in further studies aimed at confirming the long-term operational reliability of the products.

CONCLUSIONS

1. The parameters of the additive electron beam process significantly influence the shape formation quality of thin-walled products. Elevated beam travel speeds in the range of 2000–6000 mm/s lead to unstable melting and increased porosity.

2. A correlation was established between additive process parameters, surface morphology, and the level of internal defectiveness of specimens. Optimisation of printing modes substantially reduces porosity and promotes the formation of a more uniform two-phase (α+β)-structure. The best structural indicates were demonstrated by Specimen No. 8, which is distinguished by minimum defectiveness and a balanced microstructure with uniform phase distribution.

3. It was determined that chemical composition is a decisive factor in the formation of the phase state and microstructural stability of VT6 alloy. Al deficiency (<5.3 %) in Specimen No. 7 causes a shift in phase equilibrium towards the β-phase (α-Ti — 87±3 %, β-Ti — 13±3 %) and increased structural non-uniformity. Specimen No. 8, whose chemical composition meets the standard requirements, exhibits a balanced α/β ratio (α-Ti — 90±3 %, β-Ti — 10±3 %) and high crystallinity of the structure.

4. Microhardness measurements confirmed the significant influence of microstructural condition on the local mechanical properties of VT6 alloy. Specimen No. 7 is characterised by reduced and non-uniform hardness values of $HV_{0.1}$ = 1.8±0.5 GPa, attributable to phase imbalance and structural non-uniformity. Specimen No. 8 demonstrates a higher microhardness level of $HV_{0.1}$ = 3.5±0.7 GPa, corresponding to the balanced (α+β)-structure, and is consistent with characteristic values for VT6 alloy. Hardness fluctuations can be attributed to local features of the thermal cycle, which does not affect the overall structural stability.

5. The printing mode of Specimen No. 8 can be considered the most rational from the point of view of achieving the best structural condition. Application of the mode with a beam travel speed of 500 mm/s and an energy density of 40 J/mm^3 provides for thin-walled products from VT6 alloy: a dense surface, a balanced (α+β)-microstructure, and mechanical properties consistent with literature data.

FUNDING

This work was funded within the framework of the targeted scientific research programme of the National Academy of Sciences of Ukraine on the topic "Development of resource-saving electron beam and plasma-arc additive technologies for manufacturing aerospace and rocket components for military applications from high-strength titanium alloys" (state registration number 0125U000353).

ACKNOWLEDGEMENTS

The authors are grateful to High Energy Technologies LLC (Kyiv, Ukraine) for technical support in conducting the research.

REFERENCES

1. Radhika, C. et al. (2024) A review on additive manufacturing for aerospace application. *Mater. Res. Express*, 11(**2**), 022001. DOI: https://doi.org/10.1088/2053-1591/ad21ad
2. Thomas, D., Gleadall, A. (2022) Advanced metal transfer additive manufacturing of high temperature turbine blades. *Inter. J. Adv. Manuf. Technol*., **120**, 6325–6335 DOI: https://doi.org/10.1007/s00170-022-09176-2
3. Whittaker, M. (2011) *Titanium in the gas turbine engine, book advances in gas turbine technology*. 315–335, DOI: https://doi.org/10.5772/21524
4. Drummer, D., Schmidt, M. (2025) *Progress in powder based additive manufacturing*. Springer Tracts in Additive Manufacturing. eBook. DOI: https://doi.org/10.1007/978-3-031-78350-0
5. Wang, F., Williams, S., Colegrove, P. et al. (2013) Microstructure and mechanical properties of wire and arc additive manufactured Ti–6Al–4V. *Metal. Mater. Transact. A*, **44**, 968–977. DOI: https://doi.org/10.1007/s11661-012-1444-6
6. Kishor, G., Mugada, K.K., Mahto, R.P. (2025) Wire arc additive manufacturing of titanium alloys for enhancing mechanical properties and grain-refinement. *Met. Mater. Inter*., **32**, 50–80. DOI: https://doi.org/10.1007/s12540-025-02004-8
7. Romero Reséndiz, L., Sánchez Cano, T., Naeem, M. et al. (2024) Mechanical and electrochemical properties comparison of additively manufactured Ti–6Al–4V alloys by electron beam melting and selective laser melting. *J. of Materials Eng. and Performance*, **33**, 9028–9038. DOI: https://doi.org/10.1007/s11665-024-09486-4
8. Matviichuk, V., Nesterenkov, V., Berdnikova, O. (2022) Determining the influence of technological parameters of the electron-beam surfacing process on quality indicators. *Eastern-European J. of Enterprise Technologies*, **1**, 21–30. DOI: https://doi.org/10.15587/1729-4061.2024.297773
9. Matviichuk, V., Nesterenkov, V., Berdnikova, O. (2024) Determining the influence of technological parameters of electron beam surfacing process on the microstructure and microhardness of Ti–6Al–4V alloy. *Eastern-European J. of Enterprise Technologies*, **1**, 15–21. DOI: https://doi.org/10.15587/1729-4061.2024.297773
10. Powder materials produced by LLC "MULTIFLEX" [in Ukrainian]. https://powdermet.com.ua/ (access date: 23.02.2026)
11. Matviichuk, V.A., Nesterenkov, V.M., Berdnikova, O.M. (2022) Additive electron beam technology for manufacture of metal products from powder materials. *The Paton Welding J.*, **2**, 16–25. DOI: https://doi.org/10.37434/tpwj2022.02.03
12. Matviichuk, V. (2025) *Additive electron-beam technologies for the production of metal products by the method of layer-by-layer melting using powder materials*: Synopsis of Thesis for Cans. of Tech. Sci. Degree. DOI: https://doi.org/10.13140/RG.2.2.26234.61129
13. Pan Wang, Wai Jack Sin, Mui Ling Sharon Nai, Jun Wei (2017) Effects of processing parameters on surface roughness of additive manufactured Ti–6Al–4V via electron beam melting. *Materials*, 10(**10**), 1121. DOI: https://doi.org/10.3390/ma10101121
14. *VT6-Grade5*.https://evek.org/vt6-vt6s-vt6ch-splav-truba.html *VT6-Grade 5* [in Russian]. https://evek.org/vt6-vt6s-vt6ch-splav-truba.html
15. Sahoo, S., Joshi, A.P., Yazar, K.U. et al. (2026) Fine-scale microstructure, elemental distribution, and dislocation substructure formation and their influence on post-deposition phase transformation in additive manufacturing of Ti–6Al–4V alloy. *J. of Materials Eng. and Performance*, **35**, 7411–7429. DOI: https://doi.org/10.1007/s11665-025-12207-0

ORCID

V.A. Matviichuk: 0000-0002-9304-6862,
V.M. Nesterenkov: 0000-0002-7973-1986,
M.O. Sysoev: 0009-0002-0654-3914

CONFLICT OF INTEREST

The Authors declare no conflict of interest

CORRESPONDING AUTHOR

V.A. Matviichuk
E.O. Paton Electric Welding Institute of the NASU
11 Kazymyr Malevych Str., 03150, Kyiv, Ukraine
E-mail: vl.matviichuk@gmail.com

SUGGESTED CITATION

V.A. Matviichuk, V.M. Nesterenkov, M.O. Sysoev (2026) Effect of process parameters of the additive electron beam process on the properties of thin-walled products from VT6 alloy. *The Paton Welding J*., **04**, 3–10.
DOI: https://doi.org/10.37434/tpwj2026.04.01

JOURNAL HOME PAGE

https://patonpublishinghouse.com/eng/journals/tpwj

Received: 23.12.2025
Received in revised form: 25.02.2026
Accepted: 11.04.2026